

A resonant inelastic x-ray scattering study of the spin and charge excitations in the overdoped superconductor $\text{La}_{1.77}\text{Sr}_{0.23}\text{CuO}_4$

C. Monney,^{1,2} T. Schmitt,¹ C. E. Matt,^{1,3} J. Mesot,^{1,4,3}
V. N. Strocov,¹ O. J. Lipscombe,⁵ S. M. Hayden,⁵ and J. Chang^{1,4,2}

¹Swiss Light Source, Paul Scherrer Institut, CH-5232 Villigen PSI, Switzerland

²Physik-Institut, Universität Zürich, Winterthurerstrasse 190, CH-8057 Zürich, Switzerland

³Laboratory for Solid State Physics, ETH Zürich, CH-8093 Zürich, Switzerland

⁴Institute for Condensed Matter Physics, École Polytechnique Fédérale de Lausanne (EPFL), CH-1015 Lausanne, Switzerland

⁵H. H. Wills Physics Laboratory, University of Bristol, Bristol, BS8 1TL, United Kingdom

We present a resonant inelastic x-ray scattering (RIXS) study of spin and charge excitations in overdoped $\text{La}_{1.77}\text{Sr}_{0.23}\text{CuO}_4$ along two high-symmetry directions. The line shape of these excitations is analyzed and they are shown to be highly overdamped. Their spectral weight and damping are found to be strongly momentum dependent. Qualitative agreement between these observations and a calculated RPA susceptibility is obtained for this overdoped compound, implying that a significant contribution to the RIXS signal stems from a continuum of charge excitations. Furthermore, this suggests that the spin-excitations in the overdoped regime can be captured qualitatively by an itinerant picture. Our calculations also predict a new low-energy spin excitation branch to exist along the nodal direction near the zone center. With the energy resolution of the present experiment, this branch is not resolvable but we show that next generation of high-resolution spectrometers will be able to test this prediction.

I. INTRODUCTION

Conventional superconductivity emerges as a result of electron-phonon interaction¹. Information about the phonon excitation spectrum (dispersions and lifetime effects²) are therefore of great importance. Similarly, for magnetic superconductors³, there is a strong interest in understanding and experimentally revealing the spin excitation spectrum. Mapping out the detailed evolution of the spin excitation spectrum across the high-temperature superconducting cuprate phase diagram, from the Mott insulator to the Fermi-liquid ground state, is hence important. Spin excitations have traditionally been studied by inelastic neutron scattering (INS)^{4,5}. Studies of high-energy spin excitations⁶ have, however, been challenged by weak neutron cross sections. Over the last decade, resonant inelastic x-ray scattering (RIXS) has developed rapidly⁷ and energy resolution now allows studies of spin excitations^{8–10}. RIXS is therefore an attractive complementary technique to neutron scattering. This has, in particular, lead to progress in understanding correlated low-dimensional $3d$ and $5d$ electron systems^{11,12}. The spin excitation spectra of insulating one- and two-dimensional cuprates have, for example, been studied by soft x-ray RIXS using the copper L_3 -edge^{12–18}. In recent years, spin excitations of doped cuprate and pnictide superconductors have also been investigated^{9,10,12,19}. These studies suggest that the high energy ($\omega > 100$ meV) spin excitation dispersion undergoes little change with doping^{12,19,20}. This is in strong contrast to the low-energy part of the spectrum (studied by INS), that has a strong dependence on impurities²¹, magnetic field^{22,23} and doping^{24,25}.

We present a systematic RIXS study of the spin and charge excitations found in overdoped $\text{La}_{2-x}\text{Sr}_x\text{CuO}_4$

(LSCO) $x = 0.23$. The line shape of these excitations is analyzed using the response function of a damped harmonic oscillator. In this fashion, their dispersion and momentum dependence of spectral weight and damping, γ , are extracted. We find that the spectral weight and damping γ are displaying a significant momentum dependence. The line shape is sharpest around the zone center, whereas the spectral weight increases upon moving towards the zone boundary. As reported for Bi-based cuprates^{15,26}, we also find a strong nodal / antinodal anisotropy of spectral weight. These observations are captured by susceptibility calculations based on the electronic band structure. The model calculation furthermore predicts a low-energy spin excitation branch, along the (π, π) -direction, which turns out to be particularly pronounced and dispersive in LSCO with $x = 0.23$ in comparison to other doped cuprates^{15,27}. Future RIXS experiments with improved energy resolution should test this prediction.

II. METHOD

High-resolution RIXS experiments were carried out at the ADvanced REsonant Spectroscopy (ADRESS) beamline^{28,29} at the Swiss Light Source (SLS) on high quality single crystalline LSCO $x = 0.23$ samples^{25,30–32}, grown by the traveling floating zone method³³. For the tetragonal crystal structure ($a = b \approx 3.8$ Å and $c \approx 13.2$ Å), we index the reciprocal space by $q = ha^* + kb^* + \ell c^*$ where \mathbf{a}^* and \mathbf{b}^* point along the Cu-O bonds. Samples were aligned *ex-situ*, using the x-ray Laue technique, in order to access the scattering planes $(h, 0, \ell)$ or (h, h, ℓ) . Cleaving was performed *in-situ* under ultra high vacuum conditions ($< 5 \times 10^{-10}$ mbar) using a standard top-post technique and the sample was

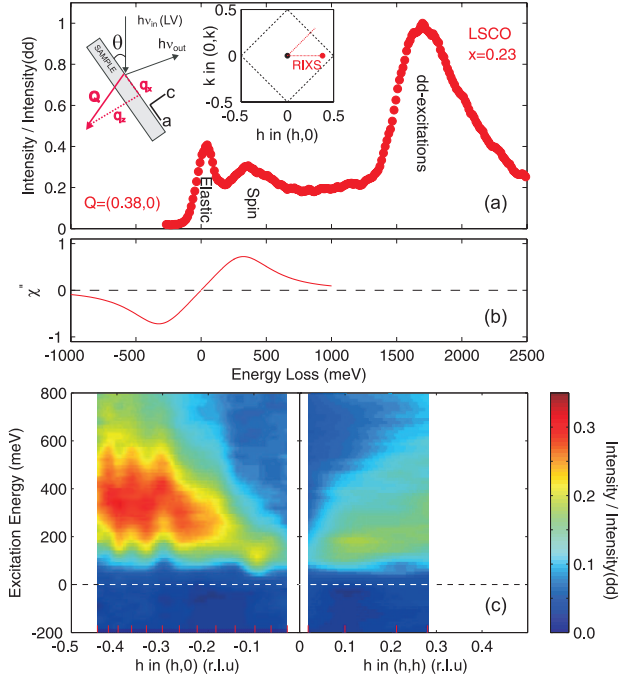


FIG. 1: (a) RIXS spectrum, recorded on overdoped LSCO $x = 0.23$ using σ -polarized light, displays elastic scattering, a low-energy excitation and a dd -excitation. The inset shows the scattering geometry and reciprocal space (h, k) schematically. (b) Overdamped response function showing how $\chi'' \rightarrow 0$ for $\omega \rightarrow 0$. (c) Interpolated RIXS intensity, with elastic scattering subtracted, versus momentum $q = (h, 0)$, (h, h) and photon energy loss ω . Red ticks indicate the grid of spectra used for the interpolation.

kept at a temperature of 20 K for all measurements. At the Cu L_3 -edge (~ 930 eV), the instrumental energy and momentum half-width-at-half-maximum (HWHM) resolutions are 65 meV and 0.01 \AA^{-1} , respectively. The incoming light was σ -polarized for all measurements. For each spectrum, the elastic line was obtained by measuring non-resonant elastic scattering from polycrystalline carbon containing tape placed just next to the sample¹⁴. Reciprocal space positions of the form $(h, 0, \ell)$ and (h, h, ℓ) were sampled by changing the grazing incident angle θ , defined in Fig. 1. The layered cuprates are known to have weak magnetic coupling along the c -axis leading to little dispersion along ℓ . We therefore describe positions using a two-dimensional notation (h, k) to quantify momentum transfer q .

III. RESULTS

A typical RIXS spectrum recorded with σ -polarized light at $(h, k) = (0.38, 0)$ is shown in Fig. 1a. As previously reported on the cuprates^{10,12,27}, the spectrum consists of three features: (1) elastic and quasi-elastic scattering at $\omega \approx 0$, (2) a low-energy excitation at around 300

meV that has been interpreted as a spin excitation in the parent compound^{9,10} and (3) so-called dd -excitations at about 1700 meV. The dd -excitations are in agreement with what has previously been reported on LSCO³⁴ and explained by crystal field calculations^{35,36}. Following common practice, all spectral intensities are renormalized to total integrated intensity of these dd -excitations, I_{dd} ^{20,27,37}.

As expected, significant elastic scattering is found near the specular condition $[q = (0, 0)]$ – see Fig. 2a. The increased elastic scattering near the grazing incidence condition $q \approx (0.4, 0)$ was previously interpreted as a result of a phonon branch¹⁰. Herein, we make no attempt to disentangle contributions from phonons and elastic scattering. We also stress that contrary to what was reported¹⁰ in underdoped LSCO $x = 0.08$, only one low-energy excitation branch is resolved in our RIXS spectra of overdoped LSCO. Hence, there is no evidence for phase separation in our compound.

A systematic compilation of RIXS spectra taken along the $(h, 0)$ and (h, h) directions are shown in Fig. 2. For simplicity only the elastic scattering and low-energy excitations are shown. In Fig. 1c, the spectral weight originating from these excitations is displayed using a false color scale and after subtracting the elastic component. Without any detailed analysis, following observations can be made. (1) Although weaker, their spectral weight remains finite in the region near the zone center $q = (0, 0)$, see Fig. 1c. (2) The spectral weight is weaker and the excitations broader and less dispersive along the (h, h) direction. A similar dichotomy between “nodal” (h, h) and “antinodal” $(h, 0)$ directions has been reported also for optimally and underdoped $\text{Bi}_2\text{Sr}_2\text{CaCu}_2\text{O}_{8+\delta}$ ^{15,26} (Bi2212). The less dispersive nodal excitation has also been reported for overdoped LSCO ($x = 0.25$)³⁸.

IV. ANALYSIS

A. Data modelling

To model the spectral weight from elastic and low-energy scattering, we use the formula $\frac{I}{I_{dd}}(\omega) = G(\omega) + n_B \chi''(\omega)$ where $n_B = (1 - \exp(\hbar\omega/k_B T))^{-1}$ accounts of the Bose factor. $G(\omega)$ is a Gaussian function (to fit the elastic line) on top of a background modeled by a cubic polynomial. The response function $\chi''(\omega)$ is that of a damped harmonic oscillator:

$$\begin{aligned} \chi''(\omega) &= \chi_0'' \frac{\gamma\omega}{[\omega^2 - \omega_0^2]^2 + \omega^2\gamma^2} \\ &= \frac{\chi_0''}{2\omega_1} \left[\frac{\gamma/2}{(\omega - \omega_1)^2 + (\gamma/2)^2} - \frac{\gamma/2}{(\omega + \omega_1)^2 + (\gamma/2)^2} \right], \end{aligned}$$

where the damping coefficient $\gamma/2 = \sqrt{\omega_0^2 - \omega_1^2}$. Considering for a moment only magnetic excitations, this response function spans two conceptually different regimes.

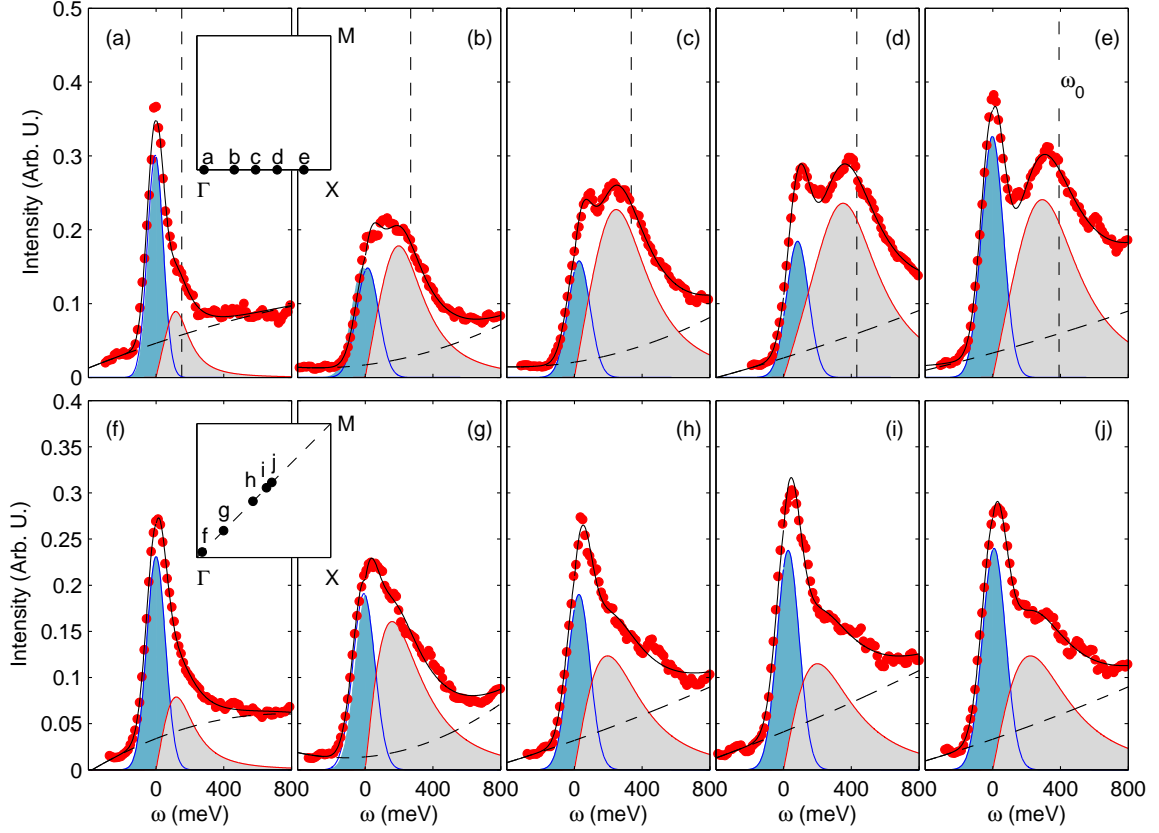


FIG. 2: RIXS spectra recorded on LSCO $x = 0.23$, at $T = 20$ K, in grazing incidence geometry using σ -polarized light tuned to the Cu L_3 -edge (930 eV) line. Top panels, (a)-(e), are spectra measured with momenta along $q = (h, 0)$ as indicated in the inset of (a). Bottom panels, (f)-(j), displays spectra taken along $q = (h, h)$ as indicated in the inset of (f)-(g). Blue and gray shaded areas are modelled contributions from elastic and low-energy excitations on top of a cubic background (dashed line). Solid black line is the sum of these contributions. See text for further explanation.

In the limit $\gamma \ll \omega_0$ ($\gamma \rightarrow 0$), $\chi'' \sim \delta(\omega - \omega_0) - \delta(\omega + \omega_0)$ describes coherent propagating magnon excitations with $\omega_0 = \omega_1$ as a pole. The overdamped limit ($\gamma \approx \omega_0$), in contrast, is characterized by $\chi'' \propto \omega$ for $\omega \rightarrow 0$ – see Fig. 1b. Furthermore, for $\omega_0 > \omega_1$, neither of these two energy scales reflect the pole of a coherent excitation. However, as χ'' is broadly peaked at ω_1 , this energy scale is often referred to as the paramagnon excitation energy scale^{12,19,37}.

Fits to spectra taken at different momenta q along $q = (h, 0)$ and (h, h) are shown in Fig. 2. Solid lines indicate the elastic (blue) and low-energy excitation (red) contributions. In this fashion γ , ω_0 , ω_1 and χ_0'' were extracted for LSCO $x = 0.23$ along the two high-symmetry directions – see Fig. 3, 4 and 5. From this analysis, it is found that $\gamma/2$ and ω_0 are comparable for all measured spectra. Interpreting the low-energy excitation along $(h, 0)$ as a spin excitation, as will be confirmed below, implies that it is overdamped. Along (h, h) , the nature of this excitation is less clear and has probably a mixed spin and charge character, which makes the interpretation of its parameters more delicate. We note that the

damping $\gamma/2$ softens upon moving from the zone boundary towards the zone center (Fig. 3b). A similar angular dependence has previously been reported in optimally doped $\text{Ba}_{0.6}\text{K}_{0.4}\text{Fe}_2\text{As}_2$ ¹⁹ (reproduced in Fig. 3a). Additionally, ω_0 disperses upward from the zone center and saturates near the zone boundary along both $(h, 0)$ and (h, h) directions. A similar dispersion of ω_1 is found along $(h, 0)$. As $\gamma/2 \approx \omega_0$, along the nodal (h, h) -direction, it is difficult to extract ω_1 reliably. Finally, we observe in Fig. 5 that the integrated intensity $\chi_0'' \cdot \gamma$ of the low-energy excitation is weakly anisotropic, as it is larger along the $(h, 0)$ direction than the (h, h) direction (for a given absolute value of the momentum $|q|$).

B. RPA susceptibility calculations

To analyze the RIXS intensities and neutron scattering spectra, itinerant approaches have been applied^{15,40–44}. These approaches are expected to be especially relevant for very overdoped cuprates, where the system enters a state with some of the characteristics of a Fermi liq-

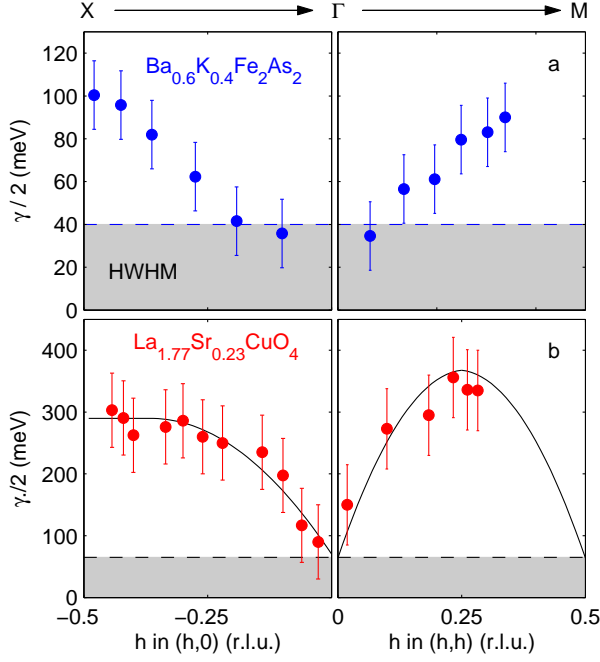


FIG. 3: Damping $\gamma/2$ (see text) of the low-energy excitations measured by RIXS in LSCO $x = 0.23$ (this work) and $\text{Ba}_{0.6}\text{K}_{0.4}\text{Fe}_2\text{As}_2$ ¹⁹ along the high-symmetry directions ΓX and ΓM . Error bars in bottom panels are set by the applied energy resolution (65 meV - HWHM) that is also indicated by a horizontal dash line.

uid^{32,45,46}. We have therefore calculated the RPA spin susceptibility $\chi_s(\mathbf{q}, \omega)$ for overdoped LSCO, to analyse the low-energy excitations in the paramagnetic state. The RPA susceptibility describes the collective magnetic excitations of the itinerant electrons. Similar to Guarise *et al.* (Ref. 15), we obtain here the transverse part of the spin susceptibility as

$$\chi_s(\mathbf{q}, \omega) = \frac{\chi_0(\mathbf{q}, \omega)}{1 - U\chi_0(\mathbf{q}, \omega)},$$

where $\chi_0(\mathbf{q}, \omega)$ represents the Lindhard response function⁴² and U is the local Coulomb interaction. As input to χ_0 , we use the single-band tight-binding parametrization⁴⁷ of the electronic dispersion obtained from ARPES measurements on this sample³⁰. The renormalized band width $4t = 490$ meV was used and U is chosen to be $1.2t$, so that the susceptibility is not diverging, meaning that the system is far enough from a density-wave instability.

In fact, the RPA susceptibility, χ_s , induces moderate modifications of the particle-hole continuum obtained from the Lindhard response function χ_0 . Along $(\pi, 0)$, the dispersion in the particle-hole continuum is renormalized to lower energies (smaller bandwidth) and starts to develop a second branch, leading to a second minimum (softening) at around $(0.15, 0)$. In this sense, it can be interpreted as a spin excitation. Along (π, π) ,

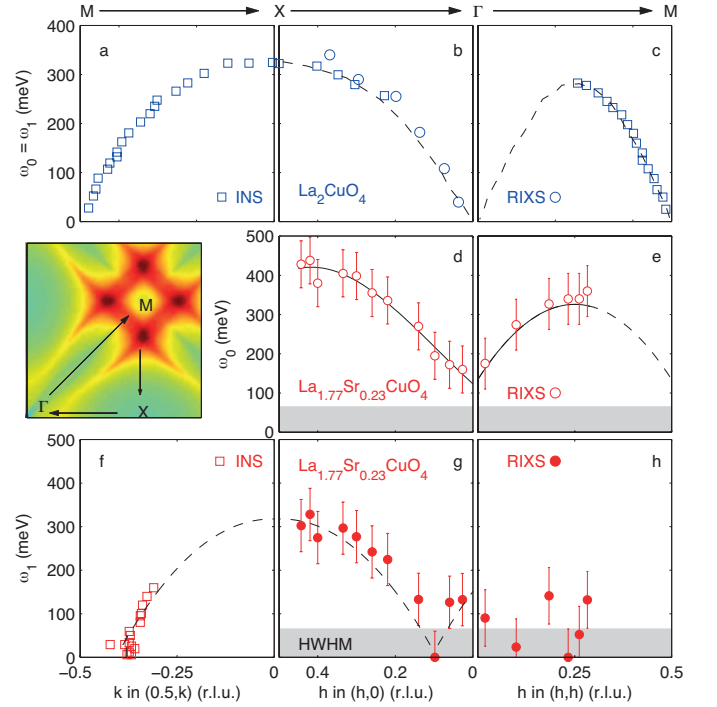


FIG. 4: Comparison of the spin excitation dispersions ω_0 and ω_1 (see text) extracted on La_2CuO_4 (LCO) with the low-energy excitation dispersions on $\text{La}_{1.77}\text{Sr}_{0.23}\text{CuO}_4$ along high symmetry directions as indicated. Data obtained from INS and RIXS are displayed by square and circular points respectively. For LCO good agreement between INS (\square - Ref. 39) and RIXS (\circ - Ref. 10) is found along the ΓX -direction. No overlap between RIXS (\bullet - this work) and INS (\square - Ref. 25) has been reached for overdoped compositions of LSCO. The inset indicates the high-symmetry directions and displays the calculated static Lindhard susceptibility (for $\omega \rightarrow 0$) (see text for further explanation).

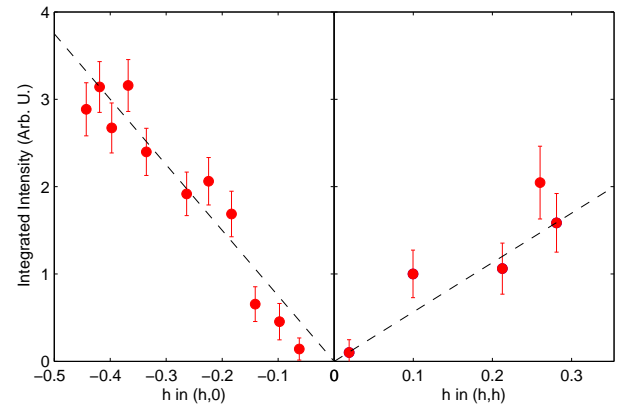


FIG. 5: Integrated intensity $\chi_0'' \cdot \gamma$ of the low-energy excitations measured by RIXS in LSCO $x = 0.23$ along the high-symmetry directions ΓX and ΓM . The dash lines are a guide to the eyes.

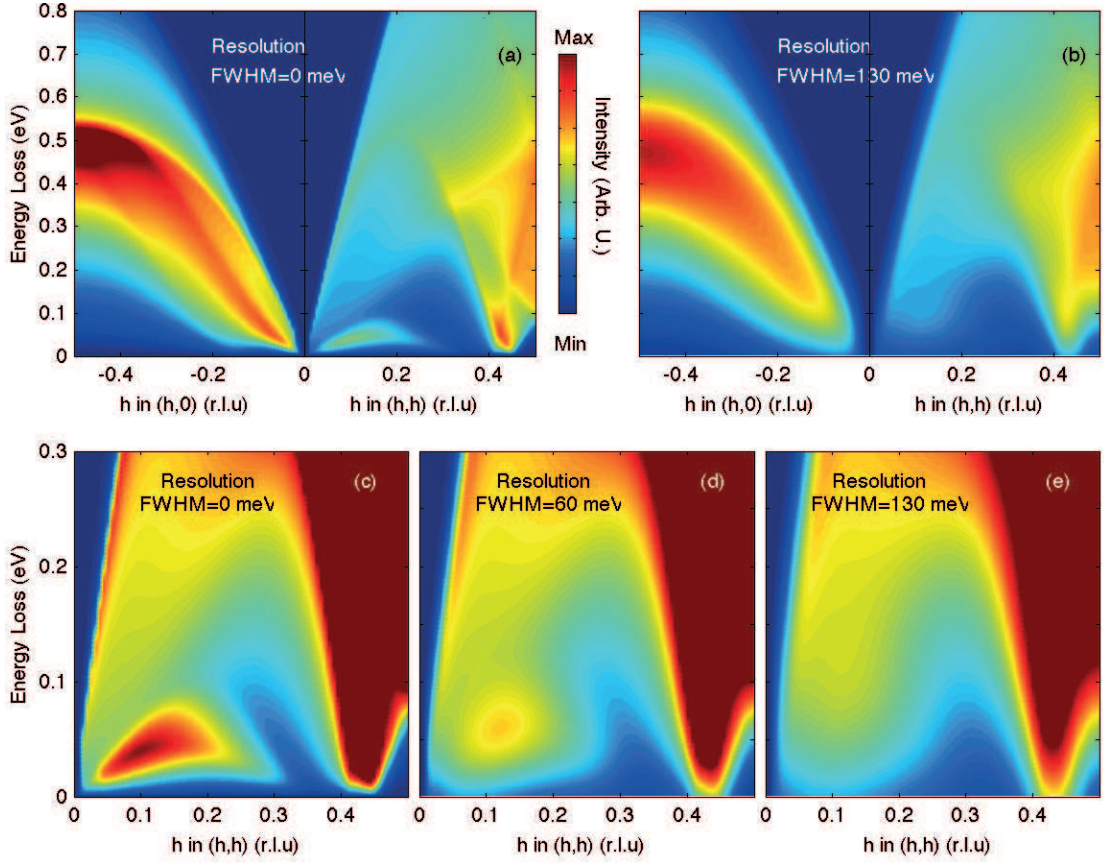


FIG. 6: (a) Calculated RPA susceptibility along the nodal (h, h) and antinodal direction $q = (h, 0)$. (b) The RPA susceptibility convolved by instrument resolution to make a direct comparison to Fig. 1c. (c-e) A zoom of the low-energy nodal RPA susceptibility. In (d,e) a Gaussian convolution with FWHM = 60 and 130 meV has been applied. This demonstrates that a spectrometer with a 60 meV energy resolution at the Cu L_3 -edge is sufficient to test the RPA prediction of low-energy nodal spin-excitations.

the main changes occur around the M -point, where low-energy spin excitations near (π, π) are reproduced consistently with previous susceptibility calculations⁴³ (see Fig. 4, inset). Interestingly, a weakly dispersing branch is found in the range $(0, 0) \rightarrow (0.2, 0.2)$, see Fig. 6a,c. As it gets stronger with increasing U , we interpret it as a spin excitation branch. Notice, however, that after convolution of the applied instrumental resolution ($\sigma = 55$ meV) these detailed features are being smeared out completely (Fig. 6b,e).

V. DISCUSSION

The calculated RPA susceptibility contains contributions from both excited particle-hole continuum and spin excitations^{15,44}. RIXS should be sensitive to both these components. The convoluted RPA calculation reproduces the most salient observations. First, along the $(\pi, 0)$ direction, the spectral weight distribution is reproduced quite successfully, compare Fig. 1c with Fig. 6b.

Moreover, the calculation also produced stronger damping as the excitations disperse towards the zone boundary. Second, the susceptibility calculation captures the intensity anisotropy between $(0, 0) \rightarrow (\pi, 0)$ and $(0, 0) \rightarrow (\pi, \pi)$. Such a clear anisotropy in the intensity distribution (see Fig. 5) had not been observed previously in other RIXS studies on doped cuprates^{15,26,38}. The susceptibility calculation furthermore makes a number of predictions, that can be tested by improving the instrumental resolution. Most notable is the low-energy excitation branch along $(0, 0) \rightarrow (\pi, \pi)$. Such a low-energy dispersion appeared already in the RPA calculated of other doped cuprates^{15,26}, but was not recognized as such, mainly because it was not as distinct as in the present case. We attribute its clear dispersive character here to the specific LSCO electronic structure that has a van Hove singularity in the antinodal region³⁰. Improving the resolution to have a Gaussian standard deviation $\sigma \sim 25$ meV (FWHM ~ 60 meV) would be sufficient to resolve this predicted low-energy branch, see Fig. 6d.

In comparison to the case of undoped cuprates^{10,12},

this analysis shows that the measured excitations in overdoped LSCO are in general broader and their width (see Fig. 3b) has a stronger momentum dependence. This most likely comes from the efficient damping of spin excitations by the electron-hole continuum, as well as from the contribution of electron-hole excitations to the RIXS signal⁴⁴.

We conclude the discussion by comparing RIXS and INS studies of LSCO^{10,38}. For the undoped compound, La₂CuO₄, INS³⁹ and RIXS¹⁰ experiments overlap along the Γ X direction and excellent agreement of the measured magnon dispersion is found (see Fig. 4). Neutron scattering experiments on doped cuprates are typically restricted – due to weak cross sections – to a much narrower range around the (0.5,0.5)-point (indexed M)^{25,48} where the so-called hour-glass spin excitation dispersion is revealed^{49–51}. The RIXS technique on the other hand has kinematic constraints limiting studies to a region centered around the Γ -point. For doped cuprates, it is thus difficult to obtain a direct overlap of RIXS and INS spectra. Within the present RPA calculation the Γ - and M -points are not equivalent. Caution should therefore be taken when comparing neutron scattering data near the M -point with RIXS data recorded around the Γ -point.

VI. CONCLUSIONS

In summary, we presented a Cu L_3 -edge RIXS study of the low-energy spin and charge excitations in overdoped La_{1.77}Sr_{0.23}CuO₄. Two high-symmetry directions $(h, 0)$ and (h, h) were investigated. Spin excitations along

(h, h) are strongly damped and the damping is displaying a significant momentum dependence – larger momentum yields larger damping. Spectral weight also has momentum dependence. Along the antinodal region more spectral weight is found near the zone boundaries and more spectral weight is found in the antinodal direction than the nodal direction. RPA susceptibility calculations starting from the experimentally observed band structure captures these trends. This suggests that the measured RIXS signal originates from a mixture of spin excitations and a continuum of charge excitations. Furthermore, based on these calculations, we predict a low-energy dispersive spin excitation branch, along the (π, π) -direction, which is particularly intense and distinct from other features in the case of La_{1.77}Sr_{0.23}CuO₄. The emerging ultra-high-resolution spectrometers will be able to test this prediction.

VII. ACKNOWLEDGEMENTS:

C. M., C. E. M. and J. C. acknowledge support by the Swiss National Science Foundation under grant number PZ00P2_154867, 200021 – 137783, PZ00P2_142434, and BSSGI0_155873. C. M. also thanks the Alexander von Humboldt Foundation and MaNEP for financial support. S. M. H. acknowledges support by the United Kingdom Engineering and Physical Science Research Council under grant number EP/J015423/1. This work was performed at the ADRESS beamline of the SLS at the Paul Scherrer Institut, Villigen PSI, Switzerland. We thank the ADRESS beamline staff for technical support.

-
- ¹ J. Bardeen, L. N. Cooper, and J. R. Schrieffer, *Phys. Rev.* **108**, 1175 (1957).
 - ² T. Keller, P. Aynajian, K. Habicht, L. Boeri, S. K. Bose, and B. Keimer, *Phys. Rev. Lett.* **96**, 225501 (2006).
 - ³ D. J. Scalapino, *Rev. Mod. Phys.* **84**, 1383 (2012).
 - ⁴ R. J. Birgeneau, C. Stock, J. M. Tranquada, and K. Yamada, *Journal of the Physical Society of Japan* **75**, 111003 (2006).
 - ⁵ M. Fujita, H. Hiraka, M. Matsuda, M. Matsuura, J. M. Tranquada, S. Wakimoto, G. Xu, and K. Yamada, *Journal of the Physical Society of Japan* **81**, 011007 (2012).
 - ⁶ S. M. Hayden, G. Aeppli, H. A. Mook, T. G. Perring, T. E. Mason, S.-W. Cheong, and Z. Fisk, *Phys. Rev. Lett.* **76**, 1344 (1996).
 - ⁷ L. J. P. Ament, M. van Veenendaal, T. P. Devereaux, J. P. Hill, and J. van den Brink, *Rev. Mod. Phys.* **83**, 705 (2011).
 - ⁸ L. J. P. Ament, G. Ghiringhelli, M. M. Sala, L. Braicovich, and J. van den Brink, *Phys. Rev. Lett.* **103**, 117003 (2009).
 - ⁹ L. Braicovich, L. J. P. Ament, V. Bisogni, F. Forte, C. Aruta, G. Balestrino, N. B. Brookes, G. M. De Luca, P. G. Medaglia, F. M. Granozio, et al., *Phys. Rev. Lett.* **102**, 167401 (2009).
 - ¹⁰ L. Braicovich, J. van den Brink, V. Bisogni, M. M. Sala, L. J. P. Ament, N. B. Brookes, G. M. De Luca, M. Salluzzo, T. Schmitt, V. N. Strocov, et al., *Phys. Rev. Lett.* **104**, 077002 (2010).
 - ¹¹ J. Kim, D. Casa, M. H. Upton, T. Gog, Y.-J. Kim, J. F. Mitchell, M. van Veenendaal, M. Daghofer, J. van den Brink, G. Khaliullin, et al., *Phys. Rev. Lett.* **108**, 177003 (2012).
 - ¹² M. L. Tacon, G. Ghiringhelli, J. Chaloupka, M. M. Sala, V. Hinkov, M. W. Haverkort, M. Minola, M. Bakr, K. J. Zhou, S. Blanco-Canosa, et al., *Nat. Phys.* **7**, 725 (2011).
 - ¹³ J. Schlappa, T. Schmitt, F. Vernay, V. N. Strocov, V. Ilakovac, B. Thielemann, H. M. Rønnow, S. Vanishri, A. Piazzalunga, X. Wang, et al., *Phys. Rev. Lett.* **485**, 8285 (2012).
 - ¹⁴ J. Schlappa, K. Wohlfeld, K. J. Zhou, M. Mourigal, M. W. Haverkort, V. N. Strocov, L. Hozoi, C. Monney, S. Nishimoto, S. Singh, et al., *Nature* **103**, 047401 (2009).
 - ¹⁵ M. Guarise, B. D. Piazza, H. Berger, E. Giannini, T. Schmitt, H. M. Rønnow, G. A. Sawatzky, J. van den Brink, D. Altenfeld, I. Eremin, et al., *Nat Commun* **5** (2014), URL <http://dx.doi.org/10.1038/ncomms6760>.
 - ¹⁶ B. Dalla Piazza, M. Mourigal, M. Guarise, H. Berger, T. Schmitt, K. J. Zhou, M. Grioni, and H. M. Rønnow, *Phys. Rev. B* **85**, 100508 (2012).
 - ¹⁷ M. Guarise, B. Dalla Piazza, M. Moretti Sala, G. Ghiringhelli, L. Braicovich, H. Berger, J. N. Hancock,

- D. van der Marel, T. Schmitt, V. N. Strocov, et al., Phys. Rev. Lett. **105**, 157006 (2010).
- ¹⁸ M. Minola, G. Dellea, H. Gretarsson, Y. Peng, Y. Lu, J. Porras, T. Loew, F. Yakhou, N. Brookes, Y. Huang, et al., Physical Review Letters **114** (2015).
 - ¹⁹ K.-J. Zhou, Y.-B. Huang, C. Monney, X. Dai, V. N. Strocov, N.-L. Wang, Z.-G. Chen, C. Zhang, P. Dai, L. Patthey, et al., Nat. Comm. **4**, 1470 (2013).
 - ²⁰ M. P. M. Dean, G. Dellea, R. S. Springell, F. Yakhou-Harris, K. Kummer, N. B. Brookes, X. Liu, Y.-J. Sun, J. Strle, T. Schmitt, et al., Nat. Mat. **12**, 1019 (2013).
 - ²¹ H. Kimura, M. Kofu, Y. Matsumoto, and K. Hirota, Phys. Rev. Lett. **91**, 067002 (2003).
 - ²² J. Chang, A. P. Schnyder, R. Gilardi, H. M. Rønnow, S. Pailhes, N. B. Christensen, C. Niedermayer, D. F. McMorro, A. Hiess, A. Stunault, et al., Phys. Rev. Lett. **98**, 077004 (2007).
 - ²³ J. Chang, N. B. Christensen, C. Niedermayer, K. Lefmann, H. M. Rønnow, D. F. McMorro, A. Schneidewind, P. Link, A. Hiess, M. Boehm, et al., Phys. Rev. Lett. **102**, 177006 (2009).
 - ²⁴ B. Vignolle, S. M. Hayden, D. F. McMorro, H. M. Rnnow, B. Lake, C. D. Frost, and T. G. Perring, Nat. Phys. **3**, 163 (2007).
 - ²⁵ O. J. Lipscombe, S. M. Hayden, B. Vignolle, D. F. McMorro, and T. G. Perring, Phys. Rev. Lett. **99**, 067002 (2007).
 - ²⁶ M. P. M. Dean, A. J. A. James, A. C. Walters, V. Bisogni, I. Jarrige, M. Hcker, E. Giannini, M. Fujita, J. Pellicari, Y. B. Huang, et al., Physical Review B **90** (2014).
 - ²⁷ M. P. M. Dean, A. J. A. James, R. S. Springell, X. Liu, C. Monney, K. J. Zhou, R. M. Konik, J. S. Wen, Z. J. Xu, G. D. Gu, et al., Phys. Rev. Lett. **110**, 147001 (2013).
 - ²⁸ G. Ghiringhelli, A. Piazzalunga, C. Dallera, G. Trezzi, L. Braicovich, T. Schmitt, V. N. Strocov, R. Betemps, L. Patthey, X. Wang, et al., Review of Scientific Instruments **77**, 113108 (2006).
 - ²⁹ V. N. Strocov, T. Schmitt, U. Flechsig, T. Schmidt, A. Imhof, Q. Chen, J. Raabe, R. Betemps, D. Zimoch, J. Krempasky, et al., J. Synchrotron Radiat. **17**, 631 (2010).
 - ³⁰ J. J. Chang, M. Månsson, S. Pailhès, T. Claesson, O. J. Lipscombe, S. M. Hayden, L. Patthey, O. Tjernberg, and J. Mesot, Nature Communications **4**:2559 (2013).
 - ³¹ J. Chang, J. S. White, M. Laver, C. J. Howell, S. P. Brown, A. T. Holmes, L. Maechler, S. Strässle, R. Gilardi, S. Gerber, et al., Phys. Rev. B **85**, 134520 (2012).
 - ³² C. G. Fatuzzo, Y. Sassa, M. Månsson, S. Pailhès, O. J. Lipscombe, S. M. Hayden, L. Patthey, M. Shi, M. Grioni, H. M. Rønnow, et al., Phys. Rev. B **89**, 205104 (2014).
 - ³³ S. Komiya, Y. Ando, X. F. Sun, and A. N. Lavrov, Phys. Rev. B **65**, 214535 (2002).
 - ³⁴ G. Ghiringhelli, N. B. Brookes, E. Annese, H. Berger, C. Dallera, M. Grioni, L. Perfetti, A. Tagliaferri, and L. Braicovich, Phys. Rev. Lett. **92**, 117406 (2004).
 - ³⁵ M. M. Sala, V. Bisogni, C. Aruta, G. Balestrino, H. Berger, N. B. Brookes, G. M. de Luca, D. D. Castro, M. Grioni, M. Guarise, et al., New Journal of Physics **13**, 043026 (2011).
 - ³⁶ M. van Veenendaal, Phys. Rev. Lett. **96**, 117404 (2006).
 - ³⁷ M. Le Tacon, M. Minola, D. C. Peets, M. Moretti Sala, S. Blanco-Canosa, V. Hinkov, R. Liang, D. A. Bonn, W. N. Hardy, C. T. Lin, et al., Phys. Rev. B **88**, 020501 (2013).
 - ³⁸ S. Wakimoto, K. Ishii, H. Kimura, M. Fujita, G. Dellea, K. Kummer, L. Braicovich, G. Ghiringhelli, L. M. Debeer-Schmitt, and G. E. Granroth, Phys. Rev. B **91**, 184513 (2015).
 - ³⁹ N. S. Headings, S. M. Hayden, R. Coldea, and T. G. Perring, Phys. Rev. Lett. **105**, 247001 (2010).
 - ⁴⁰ W. Chen and O. P. Sushkov, Phys. Rev. B **88**, 184501 (2013).
 - ⁴¹ M. R. Norman, Phys. Rev. B **63**, 092509 (2001).
 - ⁴² I. Eremin and D. Manske, Phys. Rev. Lett. **94**, 067006 (2005).
 - ⁴³ R.-H. He, M. Fujita, M. Enoki, M. Hashimoto, S. Iikubo, S.-K. Mo, H. Yao, T. Adachi, Y. Koike, Z. Hussain, et al., Phys. Rev. Lett. **107**, 127002 (2011).
 - ⁴⁴ D. Benjamin, I. Klich, and E. Demler, Phys. Rev. Lett. **112**, 247002 (2014).
 - ⁴⁵ Nakamae, S. *et al.*, Phys. Rev. B **68**, 100502 (2003).
 - ⁴⁶ B. Vignolle, A. Carrington, R. A. Cooper, M. M. J. French, A. P. Mackenzie, C. Jaudet, D. Vignolles, C. Proust, and N. E. Hussey, Nature **455**, 952 (2008).
 - ⁴⁷ E. Pavarini, I. Dasgupta, T. Saha-Dasgupta, O. Jepsen, and O. K. Andersen, Phys. Rev. Lett. **87**, 047003 (2001).
 - ⁴⁸ S. Wakimoto, K. Yamada, J. M. Tranquada, C. D. Frost, R. J. Birgeneau, and H. Zhang, Phys. Rev. Lett. **98**, 247003 (2007).
 - ⁴⁹ S. M. Hayden, H. A. Mook, P. Dai, T. G. Perring, and F. Dogan, Nature **429**, 531 (2004).
 - ⁵⁰ J. M. Tranquada, H. Woo, T. G. Perring, H. Goka, G. D. Gu, G. Xu, M. Fujita, and K. Yamada, Nature **429**, 534 (2004).
 - ⁵¹ N. B. Christensen, D. F. McMorro, H. M. Rønnow, B. Lake, S. M. Hayden, G. Aeppli, T. G. Perring, M. Mangkorntong, M. Nohara, and H. Takagi, Phys. Rev. Lett. **93**, 147002 (2004).